

## Article

# Free Vibration Analysis of Functionally Gradient Sandwich Composite Plate Embedded SMA Wires in Surface Layer

Yizhe Huang, Lin Li, Zhichao Xu, Chaopeng Li and Kuanmin Mao \*

State Key Laboratory of Digital Manufacturing Equipment and Technology, Huazhong University of Science and Technology, Wuhan 430074, China; yizhehuang@hust.edu.cn (Y.H.); lilin2017@hust.edu.cn (L.L.); xuzhichao@hust.edu.cn (Z.X.); 15927673439@163.com (C.L.)

\* Correspondence: maokm@hust.edu.cn

Received: 11 May 2020; Accepted: 2 June 2020; Published: 5 June 2020



**Abstract:** In this paper, a new type of composite gradient sandwich plate structure is proposed, which embeds the pre-strained shape memory alloy (SMA) into the surface layer and the core layer composed of epoxy resin and graphite-reinforced materials. In the core layer, graphite-reinforced material has a continuous gradient distribution along the thickness direction of the sandwich plate. Dynamic behavior of composite gradient sandwich plate in thermal environment is investigated. The equations of motion and frequency equation are derived based on the Reddy shear deformation theory and the constitutive equation for a composite sandwich plate, via the Hamilton principle. Some analytical study is depicted to provide an insight into the effects of volume fraction of material composition, gradient distribution of graphite in the core layer, and pre-strain of SMA in the surface layer on the dynamic behavior of a sandwich composite plate. This study investigates the modal performance of a sandwich composite plate with two aspects, a gradient core layer of graphite-reinforced material and surface layer-embedded SMA wires, which provide a new design idea for dynamic behavior of sandwich plates.

**Keywords:** shape memory alloys; functionally gradient; sandwich composite plate; free vibration analysis

## 1. Introduction

Shape memory alloy (SMA) has various applied beneficial effects on the dynamic behavior of a plate structure due to unique material properties, especially for recovery stress characteristics and operational temperature dependence [1]. For the sandwich structure, the embedded SMA wire is generally selected on the surface sheets, which are sufficient to exert the performance of SMA. Then the core layer can use other special materials or structures to meet a variety of applicable requirements. Through embedded SMA wire in the surface sheets and unconventional design of the core layer, the modal performance of a composite sandwich plate can be synthetically adjusted in two aspects; the surface layer and the core layer. Therefore, this design concept has gradually become a new trend in the development of sandwich plates, which provides a research foundation for the avoidance of resonance and dynamic behavior control of sandwich plates.

Comprehensive research has been devoted to adjusting the stiffness of the structures through the use of SMA components. One may refer to the pioneering work on embedding SMA layers/fibers in composite structures by Rogers [2], which proposed several concepts of modification structural performance of the composite plate. In the work of Ostachowicz et al. [3], the natural frequencies of laminated composite plates were subjected to several kinds of pre-strain using the finite element

method. Integration of SMA temperature characteristics and pre-strain performance in a composite plate was further studied analytically and experimentally, which has received considerable attention in the past decades [4–7]. Shiau et al. [8–11] investigated the dynamic behavior of thermally-buckled composite plates embedded with SMA wires. In addition, among the scientific research on SMA wires applied to composite structures, more investigations have been performed into the vibration behavior of SMA composite structures, such as low velocity impact [12,13], active buckling control [14–16], thermal stability [17,18], and nonlinear free vibration response [19,20].

Modern sandwich structures consist of two very thin surface sheets, which may be embedded with SMA to give prominence to the unique property of large recoverable strain on vibration and buckling. In terms of core, honeycomb materials and polymeric foam are the mainstream choices for soft cores; simultaneously, laminated composites or functionally graded materials enhance the structural properties of the core layer in structural form [21,22]. For instance, an analytical study was carried out by Botshekanan Dehkordi et al. [23], to study the frequency of a sandwich plate with active SMA hybrid composite face sheets and a temperature-dependent flexible core. Ghaznavi et al. [24] carried out a non-linear layerwise dynamic response analysis of sandwich plates with soft auxetic cores and embedded SMA wires experiencing cyclic loadings. In another work, Nejati et al. [25] analyzed the thermal vibration of a double curved sandwich panel with embedded pre-strained SMA wires hybrid composite face sheets and a soft core. However, still fewer studies have taken into consideration the vibration analysis of sandwich structures with SMA fibers, especially the application of gradient distribution in the core layer. In this work, free vibration analysis of functionally gradient sandwich composite plate embedded SMA wires in the surface layer was investigated. According to the foregoing literature survey, novelties of the present research are that a new type of composite gradient sandwich plate structure which the core layer composed of epoxy resin and graphite-reinforced materials is proposed, and graphite acts as a functionally gradient material in the core layer. Particularly noteworthy is that the gradient parameter is used as the distribution index of graphite in the core layer under a certain content; the large modulus and distribution form of graphite are fully utilized to affect the overall rigidity of the sandwich plate. Reddy shear deformation theory is employed to improve the calculation accuracy of the mechanical properties, which doesn't require computing the shear correction factor. Then, based on SMA stress-strain relation and the Hamilton principle, we derived the governing partial differential equations of motion and frequency equation. The influence of SMA wires on the vibration behavior of a sandwich plate was examined by varying the volume fraction and pre-strain with temperature rise. The modal performance results in this study provide a theoretical basis and design concept for vibration control of a gradient sandwich composite plate with embedded SMA.

## 2. Theoretical Formula

### 2.1. Geometry and Material Properties

A schematic of the sandwich plate considered, with length  $L_a$ , width  $L_b$  and thickness  $h$  in a Cartesian coordinate system, is shown in Figure 1, in which  $h_c$  refer to the thickness of core and the thickness of top face sheet  $h_t$ ; the bottom face sheet  $h_b$  can be represented as  $h_{t(b)} = (h - h_c)/2$ . The top and bottom sheet of the composite sandwich plate were orthogonally embedded with pre-strain SMA wires respectively, while the core layer was an isotropic functionally gradient structure composed of graphite and epoxy resin.

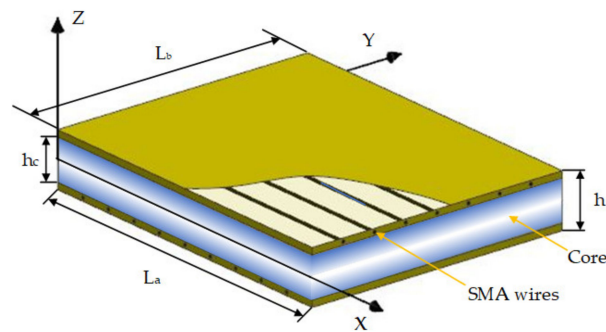


**Figure 1.** Schematic of a composite sandwich plate with functionally graded core and shape memory alloy (SMA)-composite face sheets.

The core layer of the composite sandwich plate had a symmetrical gradient distribution form. Graphite was continuously distributed in the core layer along the Z direction from the middle plane of the sandwich plate to the interface of the top (bottom) face sheet in the form of a gradient. With a certain graphite content in the core layer, the distribution of graphite tended to the outer edge of the core layer, which is a positive gradient distribution; on the contrary, the distribution of graphite tended to the central region, which is a negative gradient distribution. Non gradient distribution refers to the uniform distribution of graphite in the core layer. The distribution function of the volume fraction of graphite in the core layer can be expressed as

$$\text{Positive gradient : } V_g(z) = (p+1) \left( \frac{2|z|}{h_c} \right)^p V_g, -\frac{h_c}{2} < z < \frac{h_c}{2} \quad (1)$$

$$\text{Non gradient : } V_g(z) = V_g, -\frac{h_c}{2} < z < \frac{h_c}{2} \quad (2)$$

$$\text{Negative gradient : } V_g(z) = (p+1) \left( 1 - \frac{2|z|}{h_c} \right)^p V_g, -\frac{h_c}{2} < z < \frac{h_c}{2} \quad (3)$$

where  $p$  is the gradient index and  $p > 0$ , terms  $V_g$  and  $V_g(z)$  denote the volume fraction of graphite in the core layer and the volume fraction of graphite on Z coordinate. By applying the two-phase material mixing law, the effective Young's modulus  $E$ , Poisson's ratio  $\nu$  and density  $\bar{\rho}$ .

$$E^{(c)}(z) = E_e + (E_g - E_e)V_g(z) \quad (4)$$

$$\nu^{(c)}(z) = \nu_e + (\nu_g - \nu_e)V_g(z) \quad (5)$$

$$\bar{\rho}^{(c)}(z) = \rho_e + (\rho_g - \rho_e)V_g(z) \quad (6)$$

where subscripts 'g' and 'e' represents graphite and epoxy resin.

## 2.2. Vibration Equation

According to the Reddy shear deformation theory in a composite sandwich plate, the following assumptions are considered:

- (1) Transverse strain of sandwich plate  $\varepsilon_z = 0$ .
- (2) The straight line perpendicular to the neutral surface before deformation will no longer maintain a straight line after deformation.

The displacement caused by bending is

$$\begin{aligned} u(x, y, z, t) &= z\varphi_x(x, y, t) - \frac{4z^3}{3h^2} \left( \varphi_x(x, y, t) + \frac{\partial w(x, y, t)}{\partial x} \right) \\ v(x, y, z, t) &= z\varphi_y(x, y, t) - \frac{4z^3}{3h^2} \left( \varphi_y(x, y, t) + \frac{\partial w(x, y, t)}{\partial y} \right) \\ w(x, y, z, t) &= w(x, y, t) \end{aligned} \quad (7)$$

where  $\varphi_x(x, y, t)$ ,  $\varphi_y(x, y, t)$  are the angular displacement components along the X, Y coordinates, respectively and 'w' is the displacement components of along Z coordinate. According to the small deformation theory, the strain at any point on the outer surface of the sandwich plate can be expressed as

$$\left\{ \begin{aligned} \varepsilon_x &= z \frac{\partial \varphi_x}{\partial x} - \frac{4z^3}{3h^2} \left( \frac{\partial \varphi_x}{\partial x} + \frac{\partial^2 w}{\partial x^2} \right) \\ \varepsilon_y &= z \frac{\partial \varphi_y}{\partial y} - \frac{4z^3}{3h^2} \left( \frac{\partial \varphi_y}{\partial y} + \frac{\partial^2 w}{\partial y^2} \right) \\ \gamma_{xy} &= z \left( \frac{\partial \varphi_x}{\partial y} + \frac{\partial \varphi_y}{\partial x} \right) - \frac{4z^3}{3h^2} \left( \frac{\partial \varphi_x}{\partial y} + \frac{\partial \varphi_y}{\partial x} + 2 \frac{\partial^2 w}{\partial x \partial y} \right) \\ \gamma_{xz} &= \left( 1 - \frac{4z^2}{h^2} \right) \left( \varphi_x + \frac{\partial w}{\partial x} \right) \\ \gamma_{yz} &= \left( 1 - \frac{4z^2}{h^2} \right) \left( \varphi_y + \frac{\partial w}{\partial y} \right) \end{aligned} \right. \quad (8)$$

Assuming that the functionally gradient sandwich composite plate embedded SMA wires in surface layer shown in Figure 1 contain face sheets and core, the stress-strain relation of the kth layer can be given as [25]

$$\sigma^{(k)} = \bar{Q}^{(k)} \varepsilon^{(k)} - \sigma_T^{(k)} + k_{SMA} \sigma_r^{(k)} \quad (9)$$

where  $k$  takes  $t$ ,  $b$  and  $c$  represent the top layer, bottom layer and core layer, respectively.

$$\bar{Q}^{(k)} = \begin{bmatrix} \bar{Q}_{11}^{(k)} & \bar{Q}_{12}^{(k)} & 0 & 0 & 0 \\ \bar{Q}_{12}^{(k)} & \bar{Q}_{22}^{(k)} & 0 & 0 & 0 \\ 0 & 0 & \bar{Q}_{44}^{(k)} & 0 & 0 \\ 0 & 0 & 0 & \bar{Q}_{55}^{(k)} & 0 \\ 0 & 0 & 0 & 0 & \bar{Q}_{66}^{(k)} \end{bmatrix} \quad (10)$$

The term  $\bar{Q}^{(k)}$  denotes the modulus matrix, of which  $Q_{ij}^{(k)}$  are modulus elements. The top and bottom surfaces of the sandwich plate were orthogonal structures composed of epoxy resin embedded shape memory alloy wire, wherein the modulus element is quoted from [26]. For the gradient core,

since the elastic modulus and Poisson's ratio are both functions of the Z coordinate, and the core layer is considered to be an isotropic, the modulus matrix elements of Equation (10) are obtained as

$$\left\{ \begin{array}{l} \bar{Q}_{11}^{(c)}(z) = \bar{Q}_{22}^{(c)}(z) = \frac{E^{(c)}(z)}{1-[v^{(c)}(z)]^2} \\ \bar{Q}_{12}^{(c)}(z) = \frac{E^{(c)}(z)v^{(c)}(z)}{1-[v^{(c)}(z)]^2} \\ \bar{Q}_{66}^{(c)}(z) = \bar{G}_{12}^{(c)}(z) = \frac{E^{(c)}(z)}{2(1-v^{(c)}(z))} \\ \bar{Q}_{44}^{(c)}(z) = \bar{G}_{23}^{(c)}(z) \\ \bar{Q}_{55}^{(c)}(z) = \bar{G}_{13}^{(c)}(z) \end{array} \right. \quad (11)$$

The recovery stress induced by pre-strain of SMA and SMA coefficient are represented as  $\sigma_r^{(k)}$  and  $k_{SMA}$ , respectively, as  $k$  takes  $t$  or  $b$ . When the shape memory alloy is contained in the layer,  $k_{SMA} = 1$ , and if not,  $k_{SMA} = 0$ . The thermal stress  $\sigma_r^{(k)}$  generated by graphite and epoxy resin along the X and Y directions can be written as

$$\left\{ \begin{array}{l} (\sigma_x^T)^{(k)} = (\bar{Q}_{11}^{(k)} \alpha_x + \bar{Q}_{12}^{(k)} \alpha_y) \Delta T \\ (\sigma_y^T)^{(k)} = (\bar{Q}_{12}^{(k)} \alpha_x + \bar{Q}_{22}^{(k)} \alpha_y) \Delta T \end{array} \right. \quad (12)$$

where  $Q_{ij}^{(k)}$ ,  $\alpha$  and  $\Delta T$  indicates the modulus matrix element of the core layer, thermal expansion coefficient and the temperature difference between ambient temperature and normal temperature, respectively.

The Hamilton principle, by considering strain energy  $U$ , additional strain energy  $V$ , external work  $W$  and kinetic energy  $T$ , can be applied to derive the motion equations as

$$\int_{t_0}^{t_1} [\delta T - \delta(U + V) + \delta W] dt = 0 \quad (13)$$

where,  $\delta$  and  $t$  are variation operator and time coordinate respectively, which the latter one changes between interval  $t_0$  to  $t_1$ . According to Equation (13), the equations of motion of the sandwich composite plate are derived by variational calculation of  $\varphi_x$ ,  $\varphi_y$  and  $w$  respectively.

$$\begin{aligned} \delta \varphi_x : & \left( D_{11} - \frac{8}{3h^2} F_{11} + \frac{16}{9h^4} H_{11} \right) \frac{\partial^2 \varphi_x}{\partial x^2} + \left( D_{66} - \frac{4}{3h^2} F_{66} + \frac{16}{9h^4} H_{66} \right) \frac{\partial^2 \varphi_x}{\partial y^2} \\ & - \left( A_{44} - \frac{8}{h^2} D_{44} + \frac{16}{h^4} F_{44} \right) \varphi_x \\ & + \left( D_{12} - \frac{8}{3h^2} F_{12} + D_{66} - \frac{8}{3h^2} F_{66} + \frac{16}{9h^4} H_{66} \right) \frac{\partial^2 \varphi_y}{\partial x \partial y} \\ & + \left( -\frac{4}{3h^2} F_{11} + \frac{16}{9h^4} H_{11} \right) \frac{\partial^3 w}{\partial x^3} \\ & + \left( -\frac{4}{3h^2} F_{11} + \frac{16}{9h^4} H_{12} - \frac{8}{3h^2} F_{66} + \frac{32}{9h^4} H_{66} \right) \frac{\partial^3 w}{\partial x \partial y^2} \\ & - \left( A_{44} - \frac{8}{h^2} D_{44} + \frac{16}{h^4} F_{44} \right) \frac{\partial w}{\partial x} \\ & = \left( I_3 - \frac{8}{3h^2} I_5 + \frac{16}{9h^4} I_7 \right) \frac{\partial^2 \varphi_x}{\partial t^2} - \left( \frac{4}{3h^2} I_5 - \frac{16}{9h^4} I_7 \right) \frac{\partial^3 w}{\partial x \partial t^2} \end{aligned} \quad (14)$$

$$\begin{aligned}
\delta\varphi_y : & \left( D_{12} - \frac{8}{3h^2}F_{12} + \frac{16}{9h^4}H_{12} + D_{66} - \frac{8}{3h^2}F_{66} + \frac{16}{9h^4}H_{66} \right) \frac{\partial^2\varphi_x}{\partial x\partial y} \\
& + \left( D_{22} - \frac{8}{3h^2}F_{22} + \frac{16}{9h^4}H_{11} \right) \frac{\partial^2\varphi_y}{\partial y^2} \\
& + \left( D_{66} - \frac{4}{3h^2}F_{66} + \frac{16}{9h^4}H_{66} \right) \frac{\partial^2\varphi_y}{\partial x^2} - \left( A_{55} - \frac{8}{h^2}D_{55} + \frac{16}{h^4}F_{55} \right) \varphi_y \\
& + \left( -\frac{4}{3h^2}F_{11} + \frac{16}{9h^4}H_{12} - \frac{8}{3h^2}F_{66} + \frac{32}{9h^4}H_{66} \right) \frac{\partial^3 w}{\partial x^2\partial y} \\
& + \left( -\frac{4}{3h^2}F_{22} + \frac{16}{9h^4}H_{22} \right) \frac{\partial^3 w}{\partial y^3} - \left( A_{55} - \frac{8}{h^2}D_{55} + \frac{16}{h^4}F_{55} \right) \frac{\partial w}{\partial y} \\
& = \left( I_3 - \frac{8}{3h^2}I_5 + \frac{16}{9h^4}I_7 \right) \frac{\partial^2\varphi_y}{\partial t^2} - \left( \frac{4}{3h^2}I_5 - \frac{16}{9h^4}I_7 \right) \frac{\partial^3 w}{\partial y\partial t^2}
\end{aligned} \tag{15}$$

$$\begin{aligned}
\delta w : & - \left( -\frac{4}{3h^2}F_{11} + \frac{16}{9h^4}H_{11} \right) \frac{\partial^3\varphi_x}{\partial x^3} \\
& - \left( -\frac{4}{3h^2}F_{12} + \frac{16}{9h^4}H_{12} - \frac{8}{3h^2}F_{66} + \frac{32}{9h^4}H_{66} \right) \frac{\partial^3\varphi_x}{\partial x\partial y^2} \\
& + \left( A_{44} - \frac{8}{h^2}D_{44} + \frac{16}{h^4}F_{44} \right) \frac{\partial^2\varphi_x}{\partial x} \\
& - \left( -\frac{4}{3h^2}F_{12} + \frac{16}{9h^4}H_{12} - \frac{8}{3h^2}F_{66} + \frac{32}{9h^4}H_{66} \right) \frac{\partial^3\varphi_y}{\partial x^2\partial y} \\
& - \left( -\frac{4}{3h^2}F_{22} + \frac{16}{9h^4}H_{22} \right) \frac{\partial^3\varphi_y}{\partial y^3} + \left( A_{55} - \frac{8}{h^2}D_{55} + \frac{16}{h^4}F_{55} \right) \frac{\partial^2\varphi_y}{\partial y} \\
& - \frac{16}{9h^4}H_{11} \frac{\partial^4 w}{\partial x^4} - \frac{32}{9h^4}(H_{12} + 2H_{66}) \frac{\partial^4 w}{\partial x^2\partial y^2} - \frac{16}{9h^4}H_{22} \frac{\partial^4 w}{\partial y^4} \\
& + \left( A_{44} - \frac{8}{h^2}D_{44} + \frac{16}{h^4}F_{44} \right) \frac{\partial^2 w}{\partial x^2} + \left( A_{55} - \frac{8}{h^2}D_{55} + \frac{16}{h^4}F_{55} \right) \frac{\partial^2 w}{\partial y^2} \\
& + \left( N_x^r - N_x^T - N_x^{cT} \right) \frac{\partial^2 w}{\partial x^2} + \left( N_y^r - N_y^T - N_y^{cT} \right) \frac{\partial^2 w}{\partial y^2} + q \\
& = \left( \frac{4}{3h^2}I_5 - \frac{16}{9h^4}I_7 \right) \frac{\partial^3\varphi_x}{\partial x\partial t^2} + \left( \frac{4}{3h^2}I_5 - \frac{16}{9h^4}I_7 \right) \frac{\partial^3\varphi_y}{\partial y\partial t^2} + I_1 \frac{\partial^2 w}{\partial t^2} \\
& - \frac{16}{9h^4}I_7 \left( \frac{\partial^4 w}{\partial x^2\partial t^2} + \frac{\partial^4 w}{\partial y^2\partial t^2} \right)
\end{aligned} \tag{16}$$

where,  $q$ ,  $A$ ,  $D$ ,  $F$ ,  $H$  and  $I$  are the transverse load, stiffness terms and inertia terms, respectively;  $N^r$ ,  $N^T$ , and  $N^{cT}$  represent SMA recovery stress resultants, surface thermal stress resultants and core thermal stress resultants, respectively, which are all defined as

$$\begin{aligned}
(A_{ij}, D_{ij}, F_{ij}, H_{ij}) &= \int_{-h_c/2}^{h_c/2} \widetilde{Q}_{ij}^{(c)}(z) (1, z^2, z^4, z^6) dz + \int_{h_c/2}^{h/2} \widetilde{Q}_{ij}^{(t)}(1, z^2, z^4, z^6) dz \\
&+ \int_{-h/2}^{-h_c/2} \widetilde{Q}_{ij}^{(b)}(1, z^2, z^4, z^6) dz \quad (i, j = 1, 2, 4, 5, 6)
\end{aligned} \tag{17}$$

$$\begin{aligned}
(I_1, I_3, I_5, I_7) &= \int_{-h_c/2}^{h_c/2} \overline{\rho}^{(c)}(z) (1, z^2, z^4, z^6) dz + \int_{h_c/2}^{h/2} \overline{\rho}^{(t)}(1, z^2, z^4, z^6) dz \\
&+ \int_{-h/2}^{-h_c/2} \overline{\rho}^{(b)}(1, z^2, z^4, z^6) dz
\end{aligned} \tag{18}$$

$$\begin{Bmatrix} N_x^T \\ N_y^T \end{Bmatrix} = \sum_{k=t,b} \begin{bmatrix} \bar{Q}_{11}^{(k)} & \bar{Q}_{12}^{(k)} \\ \bar{Q}_{12}^{(k)} & \bar{Q}_{22}^{(k)} \end{bmatrix} \begin{Bmatrix} \alpha_x \\ \alpha_y \end{Bmatrix}^{(k)} \Delta T h_k \quad (19)$$

$$\begin{Bmatrix} N_x^r \\ N_y^r \end{Bmatrix} = \sum_{k=t,b} \begin{Bmatrix} \sigma_x^r \\ \sigma_y^r \end{Bmatrix}^{(k)} h_k \quad (20)$$

$$\begin{Bmatrix} N_x^{cT} \\ N_y^{cT} \end{Bmatrix} = \int_{-h_c/2}^{h_c/2} \begin{bmatrix} \bar{Q}_{11}^{(c)}(z) & \bar{Q}_{12}^{(c)}(z) \\ \bar{Q}_{12}^{(c)}(z) & \bar{Q}_{22}^{(c)}(z) \end{bmatrix} \begin{Bmatrix} \alpha_x \\ \alpha_y \end{Bmatrix}^{(c)} \Delta T dz \quad (21)$$

For the simply supported square/rectangle functionally gradient plate, the boundary conditions and the state variables are assumed as

$$\begin{cases} w = \varphi_y = 0 \text{ at } x = 0, L_a \\ w = \varphi_x = 0 \text{ at } y = 0, L_b \end{cases} \quad (22)$$

$$\begin{cases} \varphi_x(x, y, t) = \sum_{m=1}^{\infty} \sum_{n=1}^{\infty} \Phi_{xmn} \cos \frac{m\pi x}{L_a} \sin \frac{n\pi y}{L_b} e^{j\omega t} \\ \varphi_y(x, y, t) = \sum_{m=1}^{\infty} \sum_{n=1}^{\infty} \Phi_{ymn} \sin \frac{m\pi x}{L_a} \cos \frac{n\pi y}{L_b} e^{j\omega t} \\ w(x, y, t) = \sum_{m=1}^{\infty} \sum_{n=1}^{\infty} W_{mn} \sin \frac{m\pi x}{L_a} \sin \frac{n\pi y}{L_b} e^{j\omega t} \end{cases} \quad (23)$$

where  $\Phi_{xmn}$ ,  $\Phi_{ymn}$  and  $W_{mn}$  are the Fourier expansion coefficients of the solution,  $m$  and  $n$  are the half wave numbers in the  $x$  and  $y$  directions, respectively, and  $\omega$  is the circular frequency. By substituting Equation (23) into Equations (14)–(16), the following equation can be obtained as

$$([K] - \omega^2[M])\{U\} = \{F\} \quad (24)$$

where  $\{U\} = \{\Phi_{xmn}, \Phi_{ymn}, W_{mn}\}^T$ ,  $\{F\} = \{0, 0, q\}^T$  and  $[K]$ ,  $[M]$  can be written as

$$[K] = \begin{bmatrix} K_{11} & K_{12} & K_{13} \\ K_{12} & K_{22} & K_{23} \\ K_{13} & K_{23} & K_{33} \end{bmatrix}, [M] = \begin{bmatrix} m_{11} & m_{12} & m_{13} \\ m_{21} & m_{22} & m_{23} \\ m_{31} & m_{32} & m_{33} \end{bmatrix} \quad (25)$$

in which  $K_{ij}$ ,  $m_{ij}$  are given as

$$K_{11} = \left(D_{11} - \frac{8}{3h^2}F_{11} + \frac{16}{9h^4}H_{11}\right)\left(\frac{m\pi}{L_a}\right)^2 - \left(D_{66} - \frac{4}{3h^2}F_{66} + \frac{16}{9h^4}H_{66}\right)\left(\frac{n\pi}{L_b}\right)^2 \quad (26)$$

$$+ \left(A_{44} - \frac{8}{h^2}D_{44} + \frac{16}{h^4}F_{44}\right)$$

$$K_{12} = K_{21} = \left(D_{12} - \frac{8}{3h^2}F_{12} + D_{66} - \frac{8}{3h^2}F_{66} + \frac{16}{9h^4}H_{66}\right)\left(\frac{m\pi}{L_a}\right)\left(\frac{n\pi}{L_b}\right) \quad (27)$$

$$K_{13} = K_{31} = \left(-\frac{4}{3h^2}F_{11} + \frac{16}{9h^4}H_{11}\right)\left(\frac{m\pi}{L_a}\right)^3 + \left(-\frac{4}{3h^2}F_{11} + \frac{16}{9h^4}H_{12} - \frac{8}{3h^2}F_{66} + \frac{32}{9h^4}H_{66}\right)\left(\frac{m\pi}{L_a}\right)\left(\frac{n\pi}{L_b}\right)^2 \quad (28)$$

$$+ \left(A_{44} - \frac{8}{h^2}D_{44} + \frac{16}{h^4}F_{44}\right)\left(\frac{m\pi}{L_a}\right)$$

$$K_{22} = \left(D_{22} - \frac{8}{3h^2}F_{22} + \frac{16}{9h^4}H_{11}\right)\left(\frac{n\pi}{L_b}\right)^2 + \left(D_{66} - \frac{4}{3h^2}F_{66} + \frac{16}{9h^4}H_{66}\right)\left(\frac{m\pi}{L_a}\right)^2 + \left(A_{55} - \frac{8}{h^2}D_{55} + \frac{16}{h^4}F_{55}\right) \quad (29)$$

$$K_{23} = \left(-\frac{4}{3h^2}F_{11} + \frac{16}{9h^4}H_{12} - \frac{8}{3h^2}F_{66} + \frac{32}{9h^4}H_{66}\right)\left(\frac{m\pi}{L_a}\right)^2\left(\frac{n\pi}{L_b}\right) \quad (30)$$

$$+ \left(-\frac{4}{3h^2}F_{22} + \frac{16}{9h^4}H_{22}\right)\left(\frac{n\pi}{L_b}\right)^2 + \left(A_{55} - \frac{8}{h^2}D_{55} + \frac{16}{h^4}F_{55}\right)\left(\frac{n\pi}{L_b}\right)$$

$$K_{33} = \frac{16}{9h^4}H_{11}\left(\frac{m\pi}{L_a}\right)^4 + \frac{32}{9h^4}(H_{12} + 2H_{66})\left(\frac{m\pi}{L_a}\right)^2\left(\frac{n\pi}{L_b}\right)^2 + \frac{16}{9h^4}H_{22}\left(\frac{n\pi}{L_b}\right)^4$$

$$+ \left(A_{44} - \frac{8}{h^2}D_{44} + \frac{16}{h^4}F_{44}\right)\left(\frac{m\pi}{L_a}\right)^2 + (N_x^r - N_x^T - N_x^{cT})\left(\frac{m\pi}{L_a}\right)^2 \quad (31)$$

$$+ \left(A_{55} - \frac{8}{h^2}D_{55} + \frac{16}{h^4}F_{55}\right)\left(\frac{n\pi}{L_b}\right)^2 + (N_y^r - N_y^T - N_y^{cT})\left(\frac{n\pi}{L_b}\right)^2$$

$$m_{11} = I_3 - \frac{8}{3h^2}I_5 + \frac{16}{9h^4}I_7 \quad (32)$$

$$m_{12} = m_{21} = 0 \quad (33)$$

$$m_{13} = m_{31} = -\left(\frac{4}{3h^2}I_5 - \frac{16}{9h^4}I_7\right)\left(\frac{m\pi}{L_a}\right) \quad (34)$$

$$m_{22} = I_3 - \frac{8}{3h^2}I_5 + \frac{16}{9h^4}I_7 \quad (35)$$

$$m_{23} = m_{32} = -\left(\frac{4}{3h^2}I_5 - \frac{16}{9h^4}I_7\right)\left(\frac{n\pi}{L_b}\right) \quad (36)$$

$$m_{33} = I_1 + \frac{16}{9h^4}I_7\left[\left(\frac{m\pi}{L_a}\right)^2 + \left(\frac{n\pi}{L_b}\right)^2\right] \quad (37)$$

The frequency equation of sandwich composite plate with no external excitation can be expressed as

$$\det([K] - \omega^2[M]) = 0 \quad (38)$$

and the natural frequency can be solved by the frequency equation.

### 3. Results and Discussion

#### 3.1. Verification and Materials

To verify the theoretical formula accuracy of this study, two numerical examples are described and discussed in predicting the free vibration behaviors. The first example is a fundamental frequency comparison of the simply supported square functionally gradient plate subjected to different gradient indices ( $p = 0, 0.5, 1, 2$ ) are presented in Table 1, which was taken from Benachour et al. [27] and Zhao et al. [28]. Functionally gradient materials (Al/Al<sub>2</sub>O<sub>3</sub> and Al/ZrO<sub>2</sub>) parameters, geometric parameters ( $L_a/L_b = 1$  and  $h/L_a = 0.1$ ), and non-dimensional natural frequencies form are given in [29]. Table 1 shows that the results of the present method for the core layer were in good agreement with the existing data on functionally gradient plates in the literature, which certifies the correctness of natural frequencies that was calculated by this study.

The second example is vibration analysis of a thermally hybrid composite sandwich plate, which was equipped with SMA fibers in the graphite-epoxy face sheets. The material properties of sheets and core, asymmetric stacking sequence, and geometrical parameters were taken from Samadpour et al. [30]. In accordance with Table 2, it the correctness has been verified by comparison of non-dimensional natural frequencies for sandwich composite plate-embedded SMA subjected to different SMA volume fractions and pre-strain. Thus, the present procedure has presented acceptable accuracy in the analytical method.



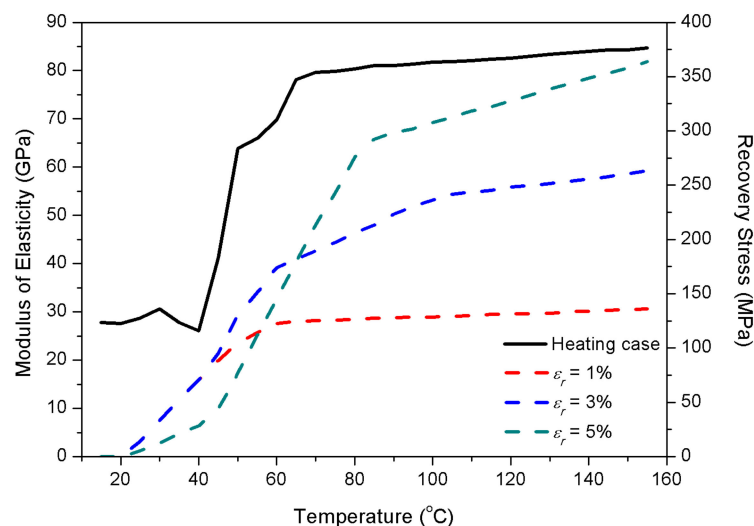
**Table 1.** Comparison of non-dimensional natural frequencies for functionally gradient plate with Benachour et al. and Zhao et al.

FGMs			Gradient Index ( $p$ )			
			0	0.5	1	2
Al/Al <sub>2</sub> O <sub>3</sub>	Benachour et al.		5.7694	4.9000	4.4166	4.0057
	Zhao et al.		5.6763	4.8209	4.3474	3.9474
	Present		5.7689	4.9123	4.4328	4.0176
Al/ZrO <sub>2</sub>	Benachour et al.		5.7694	5.4380	5.3113	5.2923
	Zhao et al.		5.6763	5.1105	4.8713	4.6977
	Present		5.7689	5.3511	5.2696	5.1254

**Table 2.** Comparison of non-dimensional natural frequencies for sandwich composite plate embedded SMA with Samadpour et al.

$V_s$ and $\varepsilon_0$	Samadpour et al.				Present			
	25 °C	35 °C	55 °C	65 °C	25 °C	35 °C	55 °C	65 °C
Without SMA	0.862	0.696	0.485	0.259	0.877	0.712	0.493	0.261
$V_s = 10\%$ $\varepsilon_0 = 2\%$	0.842	0.855	0.904	0.938	0.853	0.867	0.916	0.949
$V_s = 20\%$ $\varepsilon_0 = 2\%$	0.813	0.960	1.126	1.224	0.832	0.972	1.133	1.237
$V_s = 20\%$ $\varepsilon_0 = 1\%$	0.811	0.925	1.084	1.171	0.826	0.932	1.091	1.180
$V_s = 20\%$ $\varepsilon_0 = 0.5\%$	0.803	0.888	1.005	0.952	0.811	0.895	1.011	0.963

In the following, a composite sandwich plate with a length of 0.4 m, width of 0.3 m, and total thicknesses of 0.8 mm is considered, which core thicknesses is 0.64 mm. The plate consisted of 3 layers, of which the two outer layers are SMA/epoxy and the core layer is graphite/epoxy. The SMA wires stacking sequence of the composite face sheets were assumed as (0°/core/90°). Moreover, the martensitic phase transition to the austenitic phase is performed during the temperature rise which made the elastic modulus and recovery stress of SMA are shown in Figure 2 [31].

**Figure 2.** SMA modulus of elasticity and recovery stress vs. temperature.

In Figure 2, both elastic modulus and recovery stress of the SMA appear to have a strong temperature dependence, while recovery stress also has tensile pre-strain dependent. The material properties of the surface sheets and core are given in Table 3.

**Table 3.** Material properties of surface sheets and core.

Surface Sheets (SMA-Epoxy)			Core (Graphite-Epoxy)		
SMA		Epoxy	Graphite		
$E_s$ (GPa)	From Figure 2	$E_e$ (GPa)	3.43	$E_g$ (GPa)	275.6
$\sigma_r$ (MPa)	From Figure 2	$G_e$ (GPa)	1.27	$G_g$ (GPa)	114.8
$v_s$	0.3	$v_e$	0.35	$v_g$	0.2
$\rho_s$ (kg·m <sup>3</sup> )	6450	$\rho_e$ (kg·m <sup>3</sup> )	1250	$\rho_g$ (kg·m <sup>3</sup> )	1900
$\alpha_s$ (1/°C)	$10.26 \times 10^{-6}$	$\alpha_e$ (1/°C)	$64.80 \times 10^{-6}$	$\alpha_g$ (1/°C)	$24.40 \times 10^{-6}$

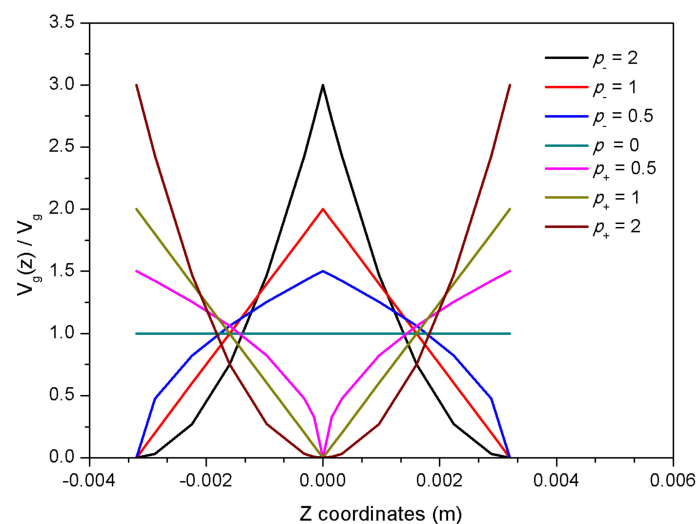
To facilitate comparison of the results of the subsequent study, the Equation (39) of the dimensionless natural frequency adopted.

$$\omega = \frac{\omega L_b^2}{2\pi h} \sqrt{\frac{\rho_e}{E_e}} \quad (39)$$

where  $E_e$  is the elastic modulus of the epoxy resin and  $\rho_e$  is the density of the epoxy resin. The terms  $\omega$  and  $\omega$  denote the dimensionless natural frequency and the natural frequency of the composite laminate, respectively.

### 3.2. Investigating the Influence of Gradient Parameter

The continuous variation of graphite in the core layer of the composite sandwich plate along the thickness direction is based on the distribution function of graphite volume fraction. There are 3 distribution forms of graphite volume fraction in the core: positive gradient distribution, uniform distribution, and negative gradient distribution. In this section, the influence of three distribution forms on the natural frequency of composite sandwich panel was comparable. The gradient parameter  $p_+/p_-$  of gradient distribution was considered to be 0.5, 1, and 2 as representative parameters of continuous gradient distribution for comparison calculation. In addition, the physical parameter  $p$  of uniform distribution was 0. Figure 3 shows the relative volume fraction of graphite along the Z coordinates reflecting the distribution function of Equation (1) to Equation (3).

**Figure 3.** The relative volume fraction of graphite along the Z coordinates.

The subscripts ‘-’ and ‘+’ of the gradient parameters represent the negative and positive gradient distribution of the graphite volume fraction respectively. The abscissa is the Z coordinate of the core layer. The vertical coordinate is the ratio of the volume fraction of graphite for unit thickness layer of Z coordinates to the volume fraction of graphite in the core layer. From the depiction in Figure 3,

the negative gradient distribution of graphite is more distributed in the central region of the core layer, while the positive gradient distribution of graphite is more distributed in the upper and lower edge regions of the core layer. The dimensionless natural frequencies vary with temperature subjected to different gradient parameter ( $p$ ) value as shown in Figure 4.

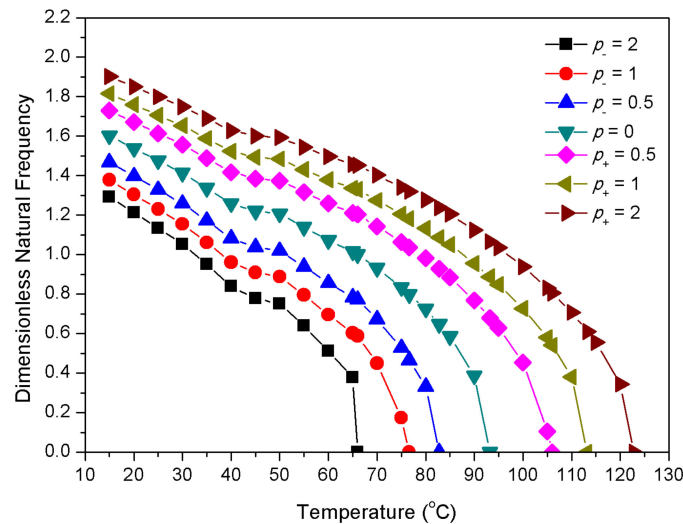


**Figure 4.** Dimensionless natural frequencies vs. temperature subjected to different gradient parameter ( $p$ ) value.

In Figure 4, the natural frequency of negative gradient distribution of graphite volume fraction is smaller than that of uniform gradient distribution, and the natural frequency of positive gradient distribution is larger than that of uniform distribution. When the distribution form shows a negative gradient, the increase in gradient parameter  $p_-$  causes the natural frequency and the critical buckling temperature to decrease. When the distribution form shows a positive gradient, the increase in the gradient parameter  $p_+$  leads to an increase in natural frequency and critical buckling temperature. With a certain total content of graphite in the core layer, the positive gradient distribution causes more graphite to distribute at the upper and lower edges of the core layer which increases the bending stiffness  $D_{ij}$  of the composite sandwich plate, while the negative gradient distribution causes more graphite to distribute at the center of the core layer which decreases the bending stiffness  $D_{ij}$ . The variation of the gradient parameter, i.e., the distribution of graphite, affects the bending stiffness of the sandwich plate, and thus the natural frequency.

Figure 5 depicts the dimensionless natural frequency of sandwich composite plate varies with positive gradient parameters ( $p_+$ ). As shown in Figure 5, the temperature was inversely proportional to the natural frequency with any gradient parameter. The reason is that with the increase of temperature, the increase of thermal stress  $N_x^{cT}$  and  $N_y^{cT}$  decreases the coefficient of bending stiffness  $K_{33}$ , which leads to the decrease of the natural frequency. At the same temperature, with the increase of positive gradient parameter, the natural frequency increases in varying degrees. At the temperature of 25 °C, 40 °C and 55 °C, the natural frequency was relatively stable as the gradient parameter increased. However, when the temperature was higher than 70 °C, the natural frequency was gradually significantly affected by the gradient parameter. Especially when the temperature was elevated and the gradient parameter decreased, the natural frequency decreased until it approached zero, at which time the sandwich plate began to buckle. In a certain temperature range and a positive gradient parameter range in Figure 5, buckling occurred only when the temperature is at 100 °C and the positive gradient parameter takes 0.2, which indicates that a higher temperature and lower gradient parameter are more prone to buckling.

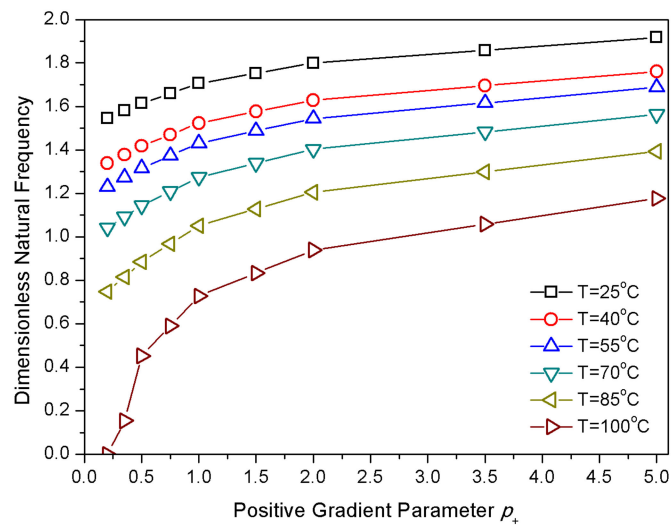


**Figure 5.** Dimensionless natural frequencies vs. the positive gradient parameter ( $p_+$ ) subjected to different temperatures.

### 3.3. Investigating the Influence of Graphite Volume Fraction

The total volume fraction of graphite in the core layer undoubtedly affects the natural frequency of the composite sandwich plate. Comparison of the natural frequencies of sandwich plates with 1% and 5% graphite volume fraction distribution in the core layer with negative gradient, uniform, and positive gradient distribution is shown in Figure 6.

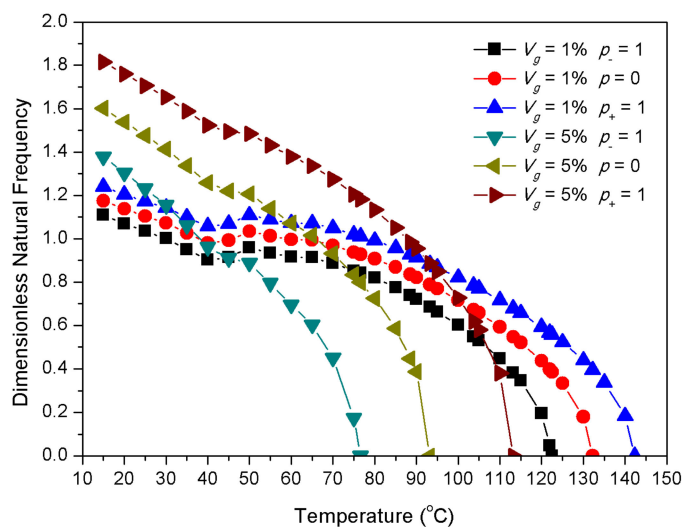


**Figure 6.** A comparison on dimensionless natural frequencies between the graphite volume fraction of 1% and 5% subjected to negative/non/positive gradient.

As can be seen in Figure 6, the natural frequency of the negative gradient distribution was less than the uniform distribution and then less than the positive gradient distribution, regardless of the volume fraction of 1% or 5%. The natural frequency of  $V_g = 5\%$  was more affected by different distribution forms than that of  $V_g = 1\%$ . This is because the increase of graphite content leads to the increase of the overall stiffness, which also magnifies the influence of gradient distribution on the sandwich plate.

At a certain gradient parameter, the natural frequency of  $V_g = 5\%$  was higher than that of  $V_g = 1\%$  in a lower temperature range. Since the stiffness of the composite sandwich plate was dominated by the modulus of graphite that the increase in the graphite content in the core layer increases the stiffness

of the sandwich plate. With the increase of temperature, the natural frequency of  $V_g = 5\%$  decreased rapidly, while the natural frequency of  $V_g = 1\%$  decreased first, then increased and then decreased slowly. This was due to the thermal stress produced by graphite in the core layer and the recovery stress produced by SMA in the surface layer playing a leading role, resulting in the rapid decline of stiffness of  $V_g = 5\%$ , while the stiffness of  $V_g = 1\%$  in the high temperature range decreased slowly and had a higher critical buckling temperature.

Figure 7 shows that the dimensionless natural frequency of a sandwich composite plate varies with graphite volume fraction. In Figure 7, the natural frequency remains relatively stable with temperature changes when the volume fraction of graphite is between 1% and 2%. With the increase of graphite volume fraction, the natural frequency is more affected by temperature. For example, in the process of temperature rising from 25 °C to 100 °C, the dimensionless natural frequency of  $V_g = 10\%$  decreased from 2.17 to 0.68, while the dimensionless natural frequency of  $V_g = 1\%$  decreased from 1.17 to 0.82. Therefore, the increase of volume fraction of graphite increases the thermal stress generated by graphite in the core layer. Then the decrease of stiffness of the sandwich plate accelerates the decrease of the natural frequency. In addition, the natural frequency increases rapidly with the increase of graphite volume fraction in the core layer at 25 °C to 55 °C, while the influence of graphite volume fraction on the natural frequency is relatively weak at 70 °C to 100 °C.

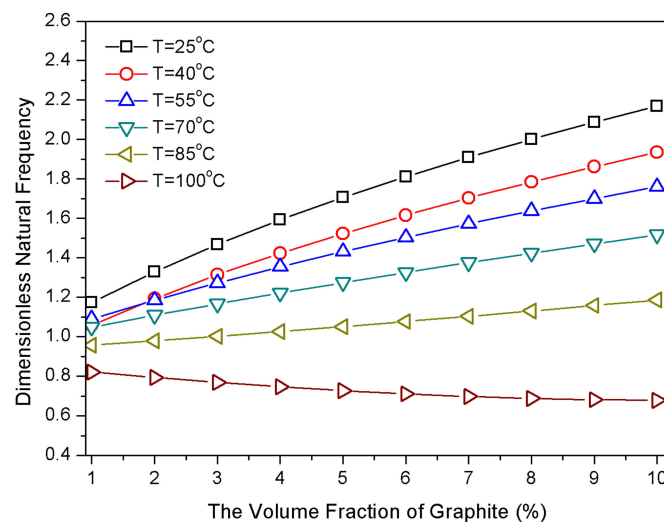


**Figure 7.** Dimensionless natural frequencies vs. the graphite volume fraction subjected to different temperature.

### 3.4. Investigating the Influence of SMA Volume Fraction

In this section, the influence of the volume fraction of SMA in the surface layer on the natural frequency of composite sandwich plate is examined. We selected 20% and 40% as representative volume fractions of SMA. In the case of negative, uniform, and positive gradient distribution of graphite in the core layer, Figure 8 analyzes the variation of the natural frequency of 20% and 40% SMA volume fraction in the surface layer with temperature.

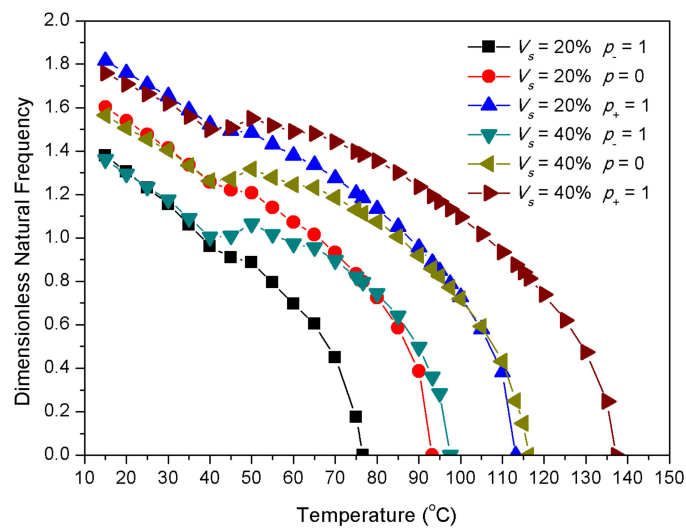


**Figure 8.** A comparison on dimensionless natural frequencies between the SMA volume fraction of 20% and 40% subjected to negative/non/positive gradient.

As shown in Figure 8, the effect of graphite distribution on natural frequency was maintained. Moreover, the volume fraction of SMA had no significant effect on the natural frequency in the temperature range of 15 °C to 40 °C. The modulus of SMA in the low temperature region was within 30GPa, so the volume fraction of SMA had no observable effect on the stiffness. Meanwhile, the recovery stress generated by the pre-strain in this process had a very weak effect on the stiffness. As the temperature was higher than 40 °C, the conversion of SMA from martensitic phase to austenitic phase lead to the rapid increase of the modulus. The stiffness of the sandwich plate with 40% SMA volume fraction was increased markedly relative to 20%. Recovery stress generated by SMA pre-strain also increased with the increase of volume fraction, so that the natural frequency of the sandwich plate increased. In addition, as the temperature rises, the natural frequency of  $V_s = 40\%$  first decreased, then increased, and then decreased to near zero. From Equation (31), it can be seen that the thermal stress decreased the stiffness, while the recovery stress increased the stiffness. The variation of natural frequency with temperature was due to the dominant role of thermal stress at 15 °C to 40 °C, while the recovery stress at 40 °C to 55 °C suddenly increased, and the thermal stress resumed its dominant role again after the temperature was higher than 55 °C.

The variations of dimensionless natural frequencies with SMA volume fraction are depicted in the Figure 9. The plot reveals that at 5% to 25% SMA volume fraction, natural frequencies decreased greatly with the increase of temperature. As the SMA volume fraction increased to 50%, the natural frequency decreased slowly with the temperature rise, that is, the dimensionless natural frequency decreased by only 0.42 during the temperature rise from 25 °C to 100 °C. This is due to the increase of the recovery stress with the increase of the volume fraction of SMA, which increased the stiffness of the sandwich plate and the natural frequency, as well as the critical buckling temperature. Therefore, the increase of SMA volume fraction reduced the difference of frequency variation of the natural frequency in the same heating process. In addition, the volume fraction of SMA had a weak effect on the natural frequency at 25 °C to 55 °C, while the natural frequency of the gradient sandwich composite plate increases with the increase of volume fraction of SMA at 70 °C to 100 °C.

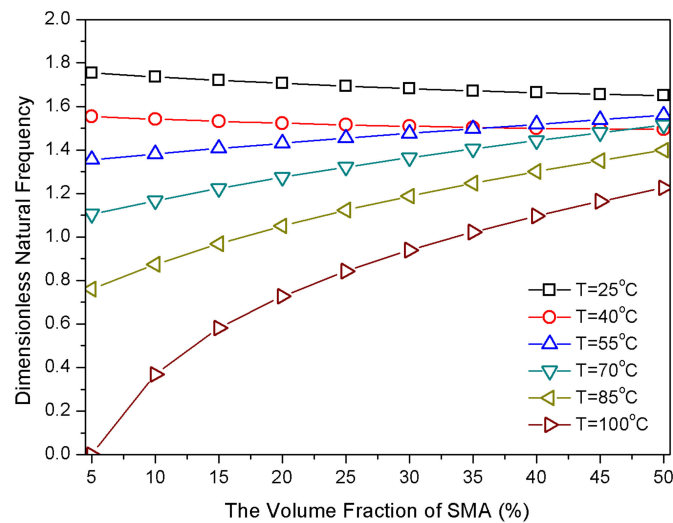


**Figure 9.** Dimensionless natural frequencies vs. the SMA volume fraction subjected to different temperatures.

### 3.5. Investigating the Influence of SMA Pre-Strain

Considering the pre-strain increment studied in this section determines the recovery stress by rising temperature, the effect of SMA pre-strain in the surface sheets for sandwich structures on natural frequency is demonstrated in Figure 10. Suppose that the volume fraction of graphite in the core layer was  $V_g = 1\%$  and distributed in the form of  $p_+ = 1$ . The representative volume fraction of the SMA volume fraction in the surface layer is 20% and 40%, respectively. A comparative study of the dimensionless frequencies was carried out, subject to the pre-strain values of 1%, 3%, and 5%.

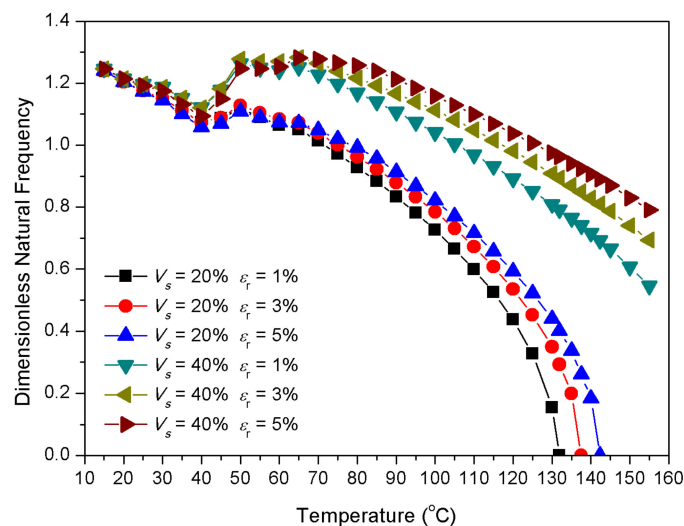


**Figure 10.** A comparison of dimensionless natural frequencies between the SMA volume fraction of 20% and 40% subjected to pre-strain 1%, 3% and 5%.

The results in Figure 10 illustrate the influence of the pre-strain of SMA on the dimensionless natural frequencies of a sandwich composite plate. As can be seen from Figure 10, neither the increment of the SMA volume fraction nor the increment of pre-strain had a significant effect on the natural frequency in the temperature range from 15 °C to 40 °C. In this temperature region, since the modulus of the SMA in the martensitic phase were about 25 MPa to 30 MPa, the increase in the volume fraction of the SMA from 20% to 40% hds a very weak influence on the stiffness. In addition, recovery stress generated by pre-strain was less than 80MPa, which had no noteworthy effect on the stiffness factor



$K_{33}$ . As the temperature rises above 40 °C, the natural frequency increases with increasing SMA volume fraction and pre-strain. Simultaneously, the critical buckling temperature could be enhanced by pre-strain increment. This is due to the martensitic phase of SMA gradually transforming to the austenitic phase during the increase of temperature, so the recovery stress generated by pre-strain increases, and the increase of volume fraction of SMA enhances the in-plane force effect, thus increasing the overall stiffness of the sandwich composite plate.

#### 4. Conclusions

From the current investigation, the following conclusions can be made:

- (1) Free vibration of a sandwich composite plate which embeds SMA wires in the surface sheets and functionally gradient distribution in the core has been developed. The constitutive equation considered thermal effect and pre-strain, the Reddy shear deformation theory, and Hamilton principle were utilized to derive the governing equations and the frequency equation.
- (2) The gradient distribution and volume fraction of graphite in the core layer of the sandwich composite plate have a significant effect on natural frequencies. The natural frequency and the critical buckling temperature of a positive gradient distribution of graphite in the core of the sandwich composite plate are higher than those of non and negative gradient distribution. Moreover, the increase of graphite volume fraction increases the natural frequency but decreases the critical buckling temperature. Therefore, the graphite in the core layer can be designed by the form of distribution and volume fraction, thereby controlling the natural frequency of sandwich plate.
- (3) Temperature-rising SMA transforms from the martensitic phase to the austenitic phase, which results in an increase in modulus and recovery stress, thus increasing the influence of the volume fraction and pre-strain on the natural frequency. Both volume fraction increments and pre-strain increments of SMA embedded in the surface sheets of the sandwich plate can increase the natural frequency and critical buckling temperature.

**Author Contributions:** Conceptualization, Y.H. and K.M.; methodology, Y.H. and Z.X.; characterization Y.H. and C.L.; writing—original draft preparation, Y.H. and L.L.; writing review and editing, Y.H. and K.M. All authors have read and agreed to the published version of the manuscript.

**Funding:** This work was financially supported by the National Natural Science Foundation of China (NSFC) under Grant Nos 51575201.

**Acknowledgments:** The authors appreciate the advice of Professor Qibai Huang (Huazhong University of Science and Technology, China).

**Conflicts of Interest:** The authors declare no conflict of interest.

#### References

1. Lagoudas, C. *Shape Memory Alloys: Modeling and Engineering Applications*; Springer: New York, NY, USA, 2007.
2. Rogers, C.; Liang, C.; Jia, J. Structural modification of simply-supported laminated plates using embedded shape memory alloy fibers. *Comput. Struct.* **1991**, *38*, 569–580. [[CrossRef](#)]
3. Ostachowicz, W.; Krawczuk, M.; Zak, A. Natural frequencies of a multilayer composite plate with shape memory alloy wires. *Finite Elem. Anal. Des.* **1999**, *32*, 71–83. [[CrossRef](#)]
4. Rogers, C.; Barker, D. Experimental studies of active strain energy tuning of adaptive composites. In Proceedings of the 31st Structures, Structural Dynamics and Materials Conference, Long Beach, CA, USA, 2–4 April 1990.
5. Rogers, C.A. Active vibration and structural acoustic control of shape memory alloy hybrid composites: Experimental results. *J. Acoust. Soc. Am.* **1990**, *88*, 2803. [[CrossRef](#)]
6. Malekzadeh, K.; Mozafari, A.; Ghasemi, F.A. Free vibration response of a multilayer smart hybrid composite plate with embedded SMA wires. *Lat. Am. J. Solids Struct.* **2014**, *11*, 279–298. [[CrossRef](#)]



7. Mahabadi, R.K.; Shakeri, M.; Daneshpazhooh, M. Free Vibration of Laminated Composite Plate with Shape Memory Alloy Fibers. *Lat. Am. J. Solids Struct.* **2016**, *13*, 314–330. [\[CrossRef\]](#)
8. Shiau, L.-C.; Wu, T.-Y. Free Vibration of Buckled Laminated Plates by Finite Element Method. *J. Vib. Acoust.* **1997**, *119*, 635–640. [\[CrossRef\]](#)
9. Shiau, L.-C.; Kuo, S.-Y.; Chang, S.-Y. Free vibration of buckled SMA reinforced composite laminates. *Compos. Struct.* **2011**, *93*, 2678–2684. [\[CrossRef\]](#)
10. Kuo, S.-Y.; Shiau, L.-C.; Chen, K.-H. Buckling analysis of shape memory alloy reinforced composite laminates. *Compos. Struct.* **2009**, *90*, 188–195. [\[CrossRef\]](#)
11. Kumar, C.N.; Singh, B.N. Thermal buckling analysis of SMA fiber-reinforced composite plates. *J. Aerosp. Eng.* **2009**, *22*, 4342. [\[CrossRef\]](#)
12. Shariyat, M.; Hosseini, S.H. Accurate eccentric impact analysis of the preloaded SMA composite plates based on a novel mixed-order hyperbolic global-local theory. *Compos. Struct.* **2015**, *124*, 140–151. [\[CrossRef\]](#)
13. Sun, M.; Wang, Z.; Yang, B. Experimental investigation of GF/epoxy laminates with different SMAs positions subjected to low-velocity impact. *Compos. Struct.* **2017**, *171*, 170–184. [\[CrossRef\]](#)
14. Choi, S.; Lee, J.-J.; Seo, D.-C. The active buckling control of laminated composite beams with embedded shape memory alloy wires. *Compos. Struct.* **1999**, *47*, 679–686. [\[CrossRef\]](#)
15. Lee, J.-J.; Choi, S. Thermal buckling and postbuckling analysis of a laminated composite beam with embedded SMA actuators. *Compos. Struct.* **1999**, *47*, 695–703. [\[CrossRef\]](#)
16. Bodaghi, M.; Shakeri, M.; Aghdam, M.-M. Thermo-mechanical behavior of shape adaptive composite plates with surface bonded shape memory alloy ribbons. *Compos. Struct.* **2015**, *119*, 115–133. [\[CrossRef\]](#)
17. Asadi, H.; Akbarzadeh, A.; Wang, Q. Nonlinear thermo-inertial instability of functionally graded shape memory alloy sandwich plates. *Compos. Struct.* **2015**, *120*, 496–508. [\[CrossRef\]](#)
18. Asadi, H.; Kiani, Y.; Aghdam, M.; Shakeri, M. Enhanced thermal buckling of laminated composite cylindrical shells with shape memory alloy. *J. Compos. Mater.* **2015**, *50*, 243–256. [\[CrossRef\]](#)
19. Park, J.-S.; Kim, J.-H.; Moon, S.-H. Vibration of thermally post-buckled composite plates embedded with shape memory alloy fibers. *Compos. Struct.* **2004**, *63*, 179–188. [\[CrossRef\]](#)
20. Li, S.-R.; Yu, W.-S.; Batra, R. Free Vibration of Thermally Pre/Post-Buckled Circular Thin Plates Embedded with Shape Memory Alloy Fibers. *J. Therm. Stresses* **2010**, *33*, 79–96. [\[CrossRef\]](#)
21. Shariyat, M.; Niknami, A. Layerwise numerical and experimental impact analysis of temperature-dependent transversely flexible composite plates with embedded SMA wires in thermal environments. *Compos. Struct.* **2016**, *153*, 692–703. [\[CrossRef\]](#)
22. Khalili, S.M.R.; Botshekanan Dehkordi, M.; Carrera, E.; Shariyat, M. Non-linear dynamic analysis of a sandwich beam with pseudoelastic SMA hybrid composite faces based on higher order finite element theory. *Compos. Struct.* **2013**, *96*, 243–255. [\[CrossRef\]](#)
23. Botshekanan Dehkordi, M.; Khalili, S.M.R. Frequency analysis of sandwich plate with active SMA hybrid composite face-sheets and temperature dependent flexible core. *Compos. Struct.* **2015**, *123*, 408–419. [\[CrossRef\]](#)
24. Ghaznavi, A.; Shariyat, M. Non-linear layerwise dynamic response analysis of sandwich plates with soft auxetic cores and embedded SMA wires experiencing cyclic loadings. *Compos. Struct.* **2017**, *171*, 185–197. [\[CrossRef\]](#)
25. Nejati, M.; Ghasemi-Ghalebahman, A.; Soltanmaleki, A. Thermal vibration analysis of SMA hybrid composite double curved sandwich panels. *Compos. Struct.* **2019**, *224*, 111035. [\[CrossRef\]](#)
26. Huang, Y.-Z.; Zhang, Z.-F.; Li, C.-P. Modal performance of two-fiber orthogonal gradient composite laminates embedded with SMA. *Materials* **2019**, *13*, 1102. [\[CrossRef\]](#)
27. Benachour, A.; Tahar, H.-D.; Atmane, H.-A. A four variable refined plate theory for free vibrations of functionally graded plates with arbitrary gradient. *Compos. Part B-Eng.* **2011**, *42*, 1186–1394. [\[CrossRef\]](#)
28. Zhao, X.; Lee, Y.-Y.; Liew, K.-M. Free vibration analysis of functionally graded plates using the element-free kp-Ritz method. *J. Sound. Vib.* **2009**, *319*, 918–939. [\[CrossRef\]](#)
29. Hosseini-Hashemi, S.-H.; Rokni Damavandi Taher, H.; Akhavan, H. Free vibration of functionally graded rectangular plates using first-order shear deformation plate theory. *Appl. Math. Modell.* **2010**, *34*, 1276–1291. [\[CrossRef\]](#)

30. Samadpour, M.; Sadighi, M.; Shakeri, M. Vibration analysis of thermally buckled SMA hybrid composite sandwich plate. *Compos. Struct.* **2015**, *119*, 251–263. [[CrossRef](#)]
31. Cross, W.-B.; Kariotis, A.-H.; Stimler, F.-J. *Nitinol Characterization Study NASA CR-1433*; National Aeronautics and Space Administration: Washington, DC, USA, 1969.



© 2020 by the authors. Licensee MDPI, Basel, Switzerland. This article is an open access article distributed under the terms and conditions of the Creative Commons Attribution (CC BY) license (<http://creativecommons.org/licenses/by/4.0/>).